LANGMUIR

Interface-Rich Materials and Assemblies

Magnetically Recyclable Fe3O4@ZnxCd1-xS Core-shell Microspheres for Visible Light Mediated Photocatalysis

Jun Zhang, Wanni Wang, Mengli Zhao, Chenyang Zhang, Chenxi Huang, Sheng Cheng, Hongmei Xu, and Haisheng Qian

Langmuir, **Just Accepted Manuscript** • DOI: 10.1021/acs.langmuir.8b01413 • Publication Date (Web): 13 Jul 2018

Magnetically Recyclable Fe_3O_4@$Zn_xCd_{1-x}S$ Core-shell Microspheres for Visible Light Mediated Photocatalysis

Jun Zhang[a], Wan-Ni Wang[a], Meng-Li Zhao[a], Chen-Yang Zhang[a], Chen-Xi Huang[a], Sheng Cheng[b], Hong-Mei Xu[a,] and Hai-Sheng Qian[a,c,*]*

[a] *Department of Medical Materials and Rehabilitation Engineering, School of Biological and Medical Engineering, Hefei University of Technology, Hefei 230009, P. R. China.*

[b] *Instrumental Analysis Center, Hefei University of Technology, Hefei 230009, P. R. China.*

[c] *Biomedical and Environmental Interdisciplinary Research Centre, Hefei, 230010, P. R. China.*

.

Correspondence should be addressed to:

Prof. H. M. Xu, E-mail: xuhongmei@hfut.edu.cn.

Prof. H. S. Qian, E-mail: shqian@hfut.edu.cn. Fax: +86 551 62901285

Abstract: Magnetically recyclable photocatalyst has drawn considerable research interest due to its importance for practical applications. Herein we demonstrate a facile hydrothermal process to fabricate magnetic core-shell microspheres of Fe_3O_4@$Zn_xCd_{1-x}S$ successfully using Fe_3O_4@ZnS core-shell microspheres as sacrificed templates. The as-prepared magnetically recyclable photocatalysts show efficient photochemical reduction of Cr(VI) under irradiation of visible light. The photochemical reduction mechanism has been studied to illustrate the reduction-oxidation ability of the photo-generated electrons (e^-) and holes (h^+); which play an important role in reduction of Cr(VI) to Cr(III) and oxidation of organic dyes. The as-prepared Fe_3O_4@$Zn_{0.55}Cd_{0.45}S$ core-shell microspheres show good chemical stability and only a slight decreasing in photocatalytic activity after four recycles. In particular, the as-prepared photocatalysts could be easily recycled and reused by an external magnetic field. Therefore, this work would provide a facile chemical approach for controlled synthesis of magnetic nanostructures combining alloyed semiconductor photocatalysts for wastewater treatment.

1. Introduction

Semiconductor photocatalysis is widely recognized as one of the most promising techniques, which can harness the solar energy directly for practical applications in solar fuels,[1-9] waste water/air treatment[10-19] and chemical synthesis.[20-24] However, catalyst-recovery for semiconductor photocatalysts is a big obstacle for their practical application.[25-26] Magnetic separation, known as the magnetic iron oxide–photocatalysts system, is widely concerned as an effective solution and it has drawn considerable research interest.[27-29] Till now, much effort has been made to fabricate magnetic recyclable composite photocatalysts, for instance, magnetic iron oxide-noble metal system,[30] including Fe_3O_4-Au,[31-32] Fe_3O_4-Ag,[33-34] Fe_3O_4-Pt,[35-36] magnetic iron oxide-graphene/graphene oxide system,[37-41] magnetic iron oxide-MOFs system,[42-45] and the magnetic iron oxide–semiconductor photocatalysis system, including Fe_3O_4-TiO_2,[46-49] Fe_3O_4-WO_3,[50] Fe_3O_4-CdS,[51-52] Fe_3O_4-MoS_2,[53] Fe_3O_4-g-C_3N_4[54-56] and so on. Recently, Huang and co-workers have successfully synthesized a unique CdS/C@Fe_3O_4 nanoreactor by the surface-imprinting technique.[57] Zuo et al have reported magnetic γ-Fe_2O_3@ZnO core-shell photocatalyst, which was firstly fabricated by hydrothermal and atomic layer deposition (ALD) method.[58] More recently, templating approach has been developed to synthesize various Fe_3O_4@void@TiO_2 yolk-shell microspheres.[59]

However, it's still a challenging work to compound incorporated magnetic nanoparticles and binary sulfide photocatalysts directly owing to large lattice mismatch between them. Additionally, single counterpart of ZnS and CdS has a weak resistance towards photo-corrosion, resulting into limiting their applications.[60-62] Compared to binary sulfide, alloyed $Zn_xCd_{1-x}S$, especially for the alloys of $Zn_{0.5}Cd_{0.5}S$ (mole ratio of Zn/Cd approximate 1.0) has been employed to be a superior substitute to avoid these drawbacks by enhancing the separated efficiency of photo-generated electrons (e^-) and holes (h^+).[63-65] To the best of our knowledge, the iron oxide-ternary semiconductor sulfide composite photocatalysis system is rarely reported.

Herein, a facile template strategy involved multi-steps has been proposed to synthesize Fe_3O_4@$Zn_xCd_{1-x}S$ core-shell microspheres (mole ratio of Zn/Cd approximate 1.0) using Fe_3O_4@ZnS

core-shell microspheres as hard template, $Cd(Ac)_2$ and thiourea used as reagents. Before that, Fe_3O_4@AA-$[Zn(OH)_4]^{2-}$ core-shell microspheres are prepared, which can be converted to Fe_3O_4@ZnS microspheres via a gaseous sulfidation process.[66] The accurate chemical composition of the mole ratio of Cd/Zn and band structure has been investigated using UV-Vis diffuse reflectance spectroscopy (DRS) and atomic absorption spectroscopy (AAS), respectively. The photochemical reduction of Cr(VI) and oxidation of organic dyes have been demonstrated under irradiation of visible light.

2. Experimental section

All chemicals were of analytic grade and used as received. The Fe_3O_4 microspheres with average size of *ca.* 300 nm were synthesized by a typical solvothermal reaction.[67]

Fabrication of Fe_3O_4@AA-$[Zn(OH)_4]^{2-}$ composite microspheres

Fe_3O_4@AA-$[Zn(OH)_4]^{2-}$ microspheres with a tunable shell thickness have been prepared via a modified procedure according to the reported protocol.[68-70] Typically, for the synthesis of Fe_3O_4@AA-$[Zn(OH)_4]^{2-}$ microspheres with 40 nm in shell thickness, 0.12mmol L-Ascorbic acid (AA) and 0.36mmol hexadecyltrimethylammonium bromide (CTAB) were dissolved using 40 mL deionized water in a flask. And then, 10mg Fe_3O_4 microspheres was added and kept stirring for 15 min. After that, 0.045 mmol of $Zn(NO_3)_2{\cdot}6H_2O$ and 0.045 mmol of hexadecyltrimethylammonium (HMTA) were added into the flask. Subsequently, the mixture solution was heated to 85 ^{o}C for 10h. Finally, the product was washed with deionized water and ethanol for several times. For comparison, Fe_3O_4@AA-$[Zn(OH)_4]^{2-}$ microspheres with shell thickness of 60 nm and 20 nm have been prepared by adding double or quarter of AA, $Zn(NO_3)_2{\cdot}6H_2O$ and HMTA. The as-prepared Fe_3O_4@AA-$[Zn(OH)_4]^{2-}$ microspheres can be converted to Fe_3O_4@ZnS microspheres via a simple gaseous sulfidation process.[66]

Synthesis of Fe_3O_4@$Zn_xCd_{1-x}S$ core-shell microspheres

Typically, 0.25 mmol cadmium acetate and 3.82 mmol thiourea and 10mg Fe_3O_4@ZnS microspheres with 40nm in shell thickness was added into 24 mL deionized water and stirred for 30 min. The mixture solution was transferred into a Teflon-lined stainless-steel autoclave (total volume is 30

mL), which was maintained at 140 °C for 1.5h. The final product was washed with deionized water and ethanol for several times and dried at 60 °C for 12h. And along with the changes of the shell thickness, the dosage was adjused to 0.11mmol cadmium acetate and 1.76 mmol thiourea for 20 nm in shell thickness and 0.37mmol cadmium acetate and 6.0 mmol thiourea for 60 nm while the other condition was kept at the same.

Photocatalytic experiments

The photocatalytic activities of as-prepared Fe_3O_4@$Zn_xCd_{1-x}S$ core-shell microspheres were evaluated by photocatalytic reduction of Cr(VI) and degradation of methylene blue (MB). Briefly, 10 mg as-prepared magnetic composite microspheres and 50 mL of Cr(VI) aqueous solution (5 mg·L^{-1}) were added into a 100 mL glass beaker and the mixed solution was shaked in dark for 1h to reach the adsorption/desorption equilibrium. Subsequently, the mixed solution was exposed to a Xe lamp (1500 mW·cm^2) with wavelength of 320–1100 nm for 35 min. 3 mL of the solution was taken out every 5 min and the catalysts were separated off by magnet. The concentration of Cr(VI) was measured by the diphenylcarbazide (DPC) method. The degradation experiments of MB were taken by the same procedure and characterized the concentration with the characteristic absorption peak at 663 nm of MB.

3. Results and Discussion

The synthetic protocol of Fe_3O_4@$Zn_xCd_{1-x}S$ core-shell microspheres involves three steps, which is illustrated in **Figure 1a**. **Figure 1b** shows the TEM image of Fe_3O_4@AA-$[Zn(OH)_4]^{2-}$ core-shell composite microspheres with 40 nm in shell thickness and the core component is with *ca.* 400 nm in diameter consistent with the size of Fe_3O_4 microspheres shown in **Figure S1a**(in the supporting information).[68-70] **Figure S1b** (in the supporting information) shows the TEM image of the Fe_3O_4@ZnS complex composite microspheres after gas sulfidation of Fe_3O_4@AA-$[Zn(OH)_4]^{2-}$ composite microspheres. **Figure 1c** shows the TEM image of the sample obtained from $Cd(Ac)_2$, thiourea and Fe_3O_4@ZnS microspheres at 140 °C for 4h; in which the product was comprised of microspheres with core-shell nanostructures. In addition, the shell component is consisted of small crystalline

nanoparticles, as revealed from the HRTEM image shown in **Figure 1d.** The lattice fringe of 3.16 Å taken from the small nanoparticle can be indexed to (101) crystal plane of $Zn_xCd_{1-x}S$ with hexagonal phase.[68] **Figure 1e-i**, STEM image and the elemental distribution mapping images of the composite microspheres demonstrate that Fe distributes in the inner component and elements of S, Zn and Cd was incorporated into the shell layer homogeneously. The merge image incorporated Zn and Fe confirmed that the Fe_3O_4@$Zn_xCd_{1-x}S$ core-shell nanostructures have been synthesized successfully.

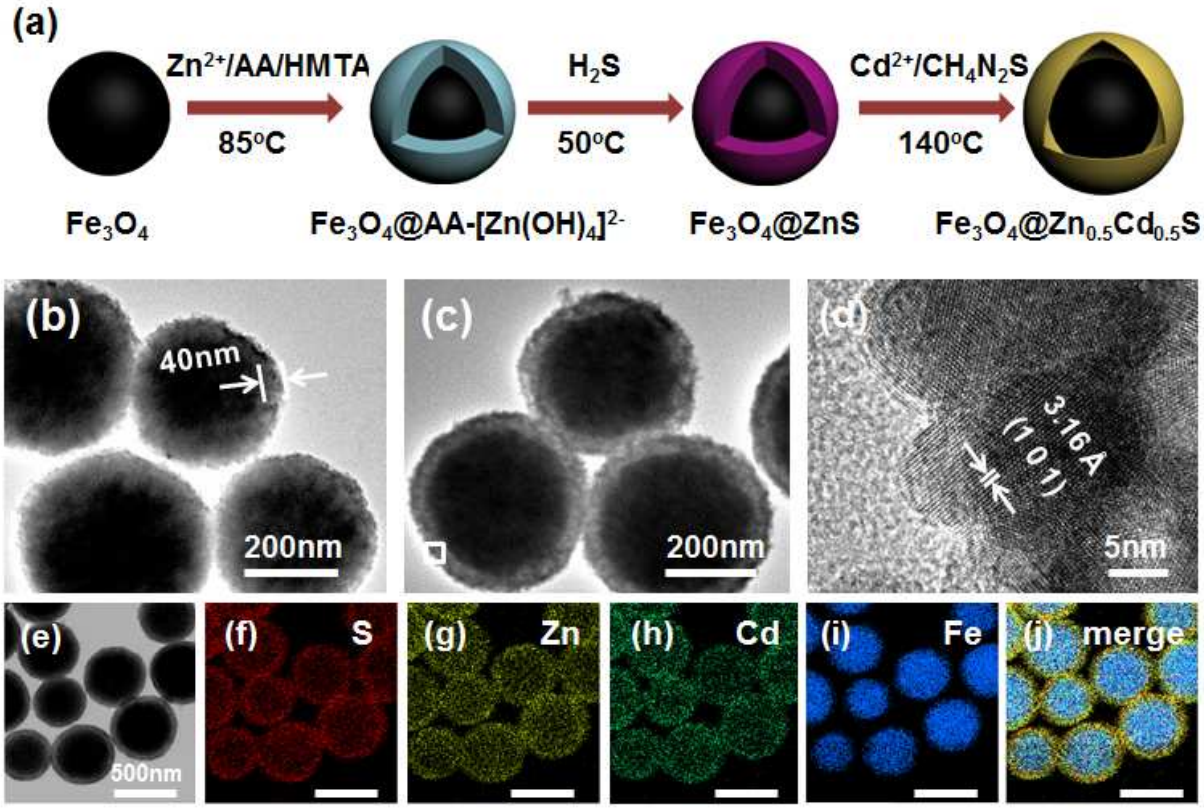

Figure 1. (a) Schematic illustration of the synthetic strategy of Fe_3O_4@$Zn_xCd_{1-x}S$ core-shell microspheres; (b) TEM image of Fe_3O_4@AA-$[Zn(OH)_4]^{2-}$ core-shell microspheres; (c,d) TEM and HRTEM images of $Zn_{0.51}Cd_{0.49}S$ core-shell microspheres; (e) STEM image of the Fe_3O_4@$Zn_{0.51}Cd_{0.59}S$ core-shell microspheres; (f-i) STEM elemental mapping images of S, Zn, Cd, Fe and merged image of the elements of Zn and Fe.

The phase and chemical composition of the Fe_3O_4@$Zn_xCd_{1-x}S$ composites have been investigated using XRD, AAS and XPS, respectively. The sharp diffraction peaks in XRD pattern shown in **Figure 2a** can be assigned to spinel ferrite (Fe_3O_4, JCPDS No. 75-1609).[71] The three wide and weak diffraction peaks are derived from the shell component. As shown in **Figure S2(in the supporting information)**,

the three Gaussian peaks located at 25.90, 26.92 and 28.22° are very fitted to the wide diffraction peaks located at 27.5°, slightly higher than that of the pure CdS, demonstrating alloyed $Zn_xCd_{1-x}S$ nanostructures formed in this work. The chemical composition calculated from EDX spectra has been shown in **Table S1 (in the supporting information).** The atomic ratio of Zn/Cd in Fe_3O_4@$Zn_xCd_{1-x}S$ is 0.51/0.49 using atomic absorption spectroscopy (AAS) (**Table S2, in the supporting information**). Thus, the Fe_3O_4@$Zn_{0.51}Cd_{0.49}S$ core-shell microspheres have been synthesized successfully via the present synthetic protocol. Moreover, the shell thickness of the as-prepared Fe_3O_4@$Zn_{0.51}Cd_{0.49}S$ core-shell microspheres can be tunable by using the Fe_3O_4@AA-$[Zn(OH)_4]^{2-}$ complex composite microspheres with different shell thickness (**Figure S3, in the supporting information**).

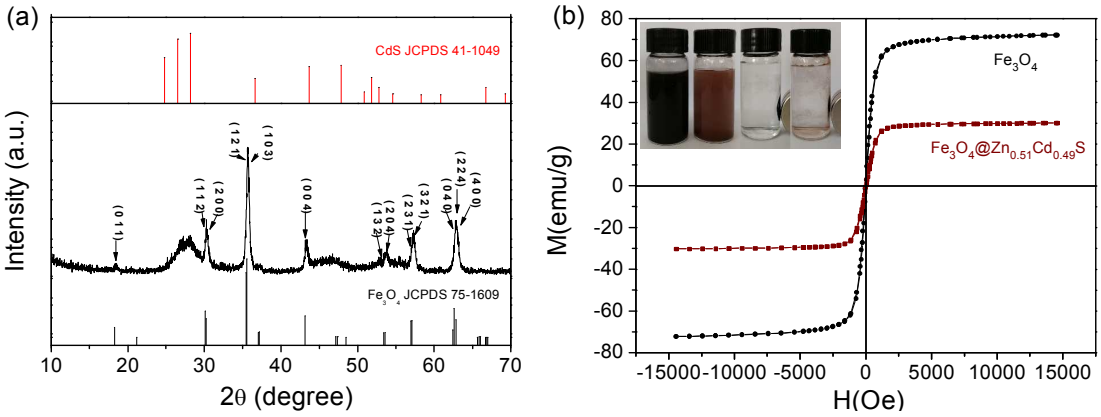

Figure 2. (a) XRD patterns of the Fe_3O_4@$Zn_{0.51}Cd_{0.49}S$ core-shell microspheres; (b) magnetic hysteresis loops of Fe_3O_4 and Fe_3O_4@$Zn_{0.51}Cd_{0.49}S$ microspheres at 300K, inset pictures showing Fe_3O_4 and Fe_3O_4@$Zn_{0.51}Cd_{0.49}S$ core-shell microspheres can be recycled from aqueous solution by an external magnetic field.

Figure 2b is the magnetic hysteresis loops of Fe_3O_4 and Fe_3O_4@$Zn_{0.51}Cd_{0.49}S$ microspheres, the Fe_3O_4@$Zn_{0.51}Cd_{0.49}S$ core-shell microspheres exhibit paramagnetic performance and the saturation magnetization reaches up to 30.15 emu/g at 300K, which is accordance with that of spinel ferrite previously reported.[71] **Figure 3a** shows a general survey of the X-ray photoelectron spectroscopy (XPS) of the Fe_3O_4@$Zn_{0.51}Cd_{0.49}S$ microspheres, verifying the co-existence of the elements including Fe, Zn, Cd, S and O elements. As shown in **Figure 3b,c**, the binding energies centered at 1044.98, 1021.98, 411.78, and 405.08 eV can be assigned to the binding energies of Zn 2p of Zn^{2+} and Cd 3d of

Cd^{2+}, respectively. The weak peaks centered at 732.08, 724.39, and 710.50 eV can be fitted to four Gaussian peaks located at 732.08, 724.39, 711.39 and 710.23 eV (**Figure 3d**), which can be assigned to the binding energy of Fe^{2+} and Fe^{3+}, confirming that the Spinel phase of Fe_3O_4 have been prepared and used in the present study.[71]

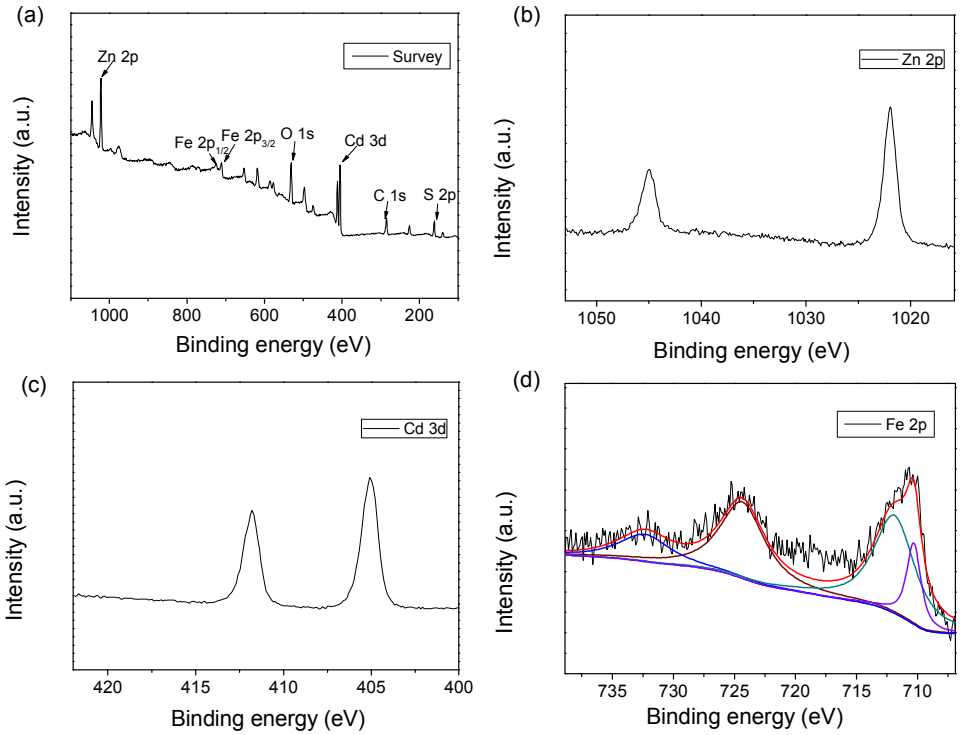

Figure 3. XPS of Fe_3O_4@$Zn_{0.51}Cd_{0.49}S$ core-shell microspheres: (a) a general survey; (b) Zn 2p; (c) Cd 3d; (d) Fe 2p; respectively.

Figure 4a shows the UV-Vis diffuse reflectance spectra (DRS) of the Fe_3O_4@$Zn_{0.51}Cd_{0.49}S$ core-shell microspheres, in which a wide absorption peak located at 470 nm has been clearly observed, which is a obviously blue-shift compared to pure CdS, indicating the formation of alloyed $Zn_xCd_{1-x}S$.[69] The band-gap energy of the Fe_3O_4@$Zn_{0.51}Cd_{0.49}S$ core-shell microspheres has been evaluated from the DRS according to the Kubelka-Munk function $[F(R)h\nu]^2$ versus photon energy ($h\nu$) (**Figure 4b**).[72] Thus, Fe_3O_4@$Zn_xCd_{1-x}S$ core-shell microspheres has been prepared successfully via the present protocol. As expected, the as-prepared Fe_3O_4@$Zn_xCd_{1-x}S$ composite microspheres with magnetic recyclability can be widely applied in wastewater treatment in the near future.

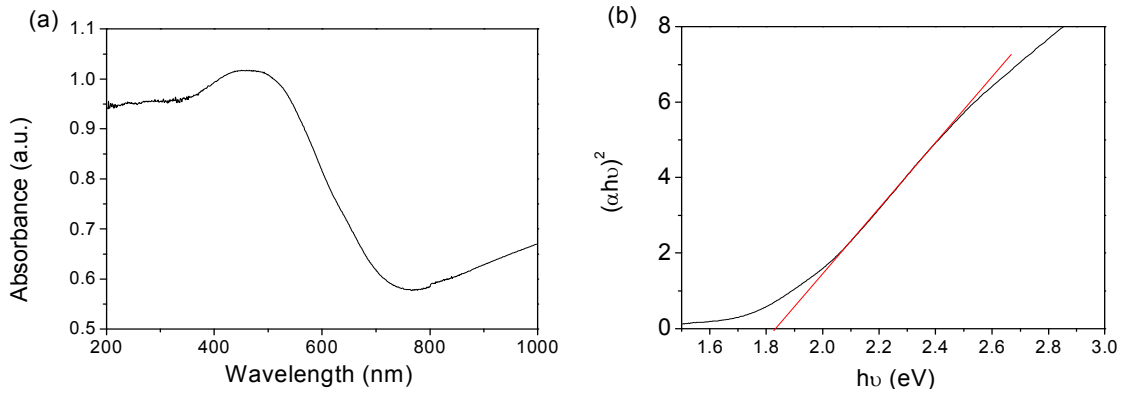

Figure 4. (a) UV–Vis diffuse reflectance spectra (DRS) of the Fe_3O_4@$Zn_{0.51}Cd_{0.49}S$ microspheres; (b) Kubelka-Munk plots used to estimate the band gap energy for the Fe_3O_4@$Zn_{0.51}Cd_{0.49}S$ microspheres. (Eg=1.83 eV).

Alloyed $Zn_xCd_{1-x}S$ nanostructures has been widely used in photocatalytic reduction or oxidation towards inorganic ions or organic dyes.[63-65] Herein Cr(VI) and methylene blue (MB) have been selected as model for investigation of the photocatalytic performance. Diphenylcarbazide (DPC) method has been widely used to analyze the concentration of Cr(VI) and evaluate the photocatalytic reduction ability for the as-prepared photocatalyst.[73-74] **Figure 5a-d** show the UV-Vis absorbance spectra of Cr(VI)-complex and digital photos of the Cr(VI) aqueous solution, demonstrating that the reduction of Cr(VI) has been efficiently realized in presence of Fe_3O_4@$Zn_{0.55}Cd_{0.45}S$ core-shell microspheres under irradiation of 1500 mW Xe lamp. In addition, the composite microspheres can be reused and recycled by a magnet. As shown in **Figure 5e, f**, more than 90 % of Cr(VI) in 50 mL aqueous solution (5 $mg \cdot L^{-1}$) can be reduced to Cr(III) using 10 mg Fe_3O_4@$Zn_{0.55}Cd_{0.45}S$ microspheres after irradiation for 35 min. As expected, the Fe_3O_4@$Zn_{0.55}Cd_{0.45}S$ microspheres obtained from Fe_3O_4@AA-$[Zn(OH)_4]^{2-}$ core-shell microspheres with 60 nm in shell thickness show the best photochemical reduction ability towards Cr(VI) than that of Fe_3O_4@$Zn_{0.51}Cd_{0.49}S$ and Fe_3O_4@$Zn_{0.55}Cd_{0.45}S$ core-shell microspheres with thinner shell thickness. Particularly, the Fe_3O_4@$Zn_xCd_{1-x}S$ composite microsphere show excellent chemical stability. As shown in **Figure 5g**, only a slight loss in photocatalytic ability for the as-prepared Fe_3O_4@$Zn_{0.51}Cd_{0.49}S$ core-shell microspheres and more than 85% of Cr(VI) was still photo-chemically reduced after four successive recycling photocatalytic experiments. Furthermore, the as-

prepared $Fe_3O_4@Zn_xCd_{1-x}S$ composite microspheres also show excellent photo-degradation towards organic dyes in aqueous solution. As shown in **Figure S4 (in the supporting information),** 92% of methylene blue (50 mL, 3.0 mg/L) in aqueous solution can be photo-oxidized in 35 min using 5 mg $Fe_3O_4@Zn_{0.55}Cd_{0.45}S$ core-shell microspheres under irradiation of the lamp after four successive recycling photocatalytic experiments. The as-prepared $Fe_3O_4@Zn_{0.55}Cd_{0.45}S$ core-shell microspheres with thicker shell thickness exhibit excellent photo-reduction and photo-oxidation ability, which may be attributed to the increasement of the photocatalyst ($Zn_{0.55}Cd_{0.45}S$) with thicker shell component. The photocurrent responses and impedance spectroscopy (EIS) of the as-prepared samples have been operated and shown in **Figure 6**, which demonstrate and confirm that the $Fe_3O_4@Zn_{0.55}Cd_{0.45}S$ core-shell microspheres possess producing more photo-generated electrons (e^-) and higher separation and migration of photo-induced charge carriers. In addition, the fluorescence spectra of 2-hydroxyl terephthalic acid shown in **Figure S5 (in the supporting information)** also show that a considerable amount of hydroxyl radical (·OH) produced excited using a Xe lamp and the as-prepared $Fe_3O_4@Zn_{0.55}Cd_{0.45}S$ core-shell microspheres shows stronger production ability of hydroxyl radicals.[75] All of these indicate that a considerable amount of photo-generated electrons and holes produced when the core-shell microspheres under irradiation. As discussed previously, the photo-generated electrons can reduce the Cr(VI) to Cr(III) and the h^+ can oxidize H_2O/O_2 to reactive oxygen species (ROS) which have strong oxidative ability and take crucial role in the photodegradation reactions and as-generated ROS can oxidize the organic dyes to carbon oxides and water.[76-79] The reaction formulas can be illustrated and summarized as follows:

$$Zn_xCd_{1-x}S + h\nu \rightarrow h^+ + e^- \quad (1)$$

$$H_2O + h^+ \rightarrow \cdot OH + H^+ \quad (2)$$

$$Cr_2O_7^{2-} + 14H^+ + 6e^- \rightarrow 2Cr^{3+} + 7H_2O \quad (3)$$

$$ROS + dye \rightarrow \ldots \rightarrow CO_2 + H_2O \quad (4)$$

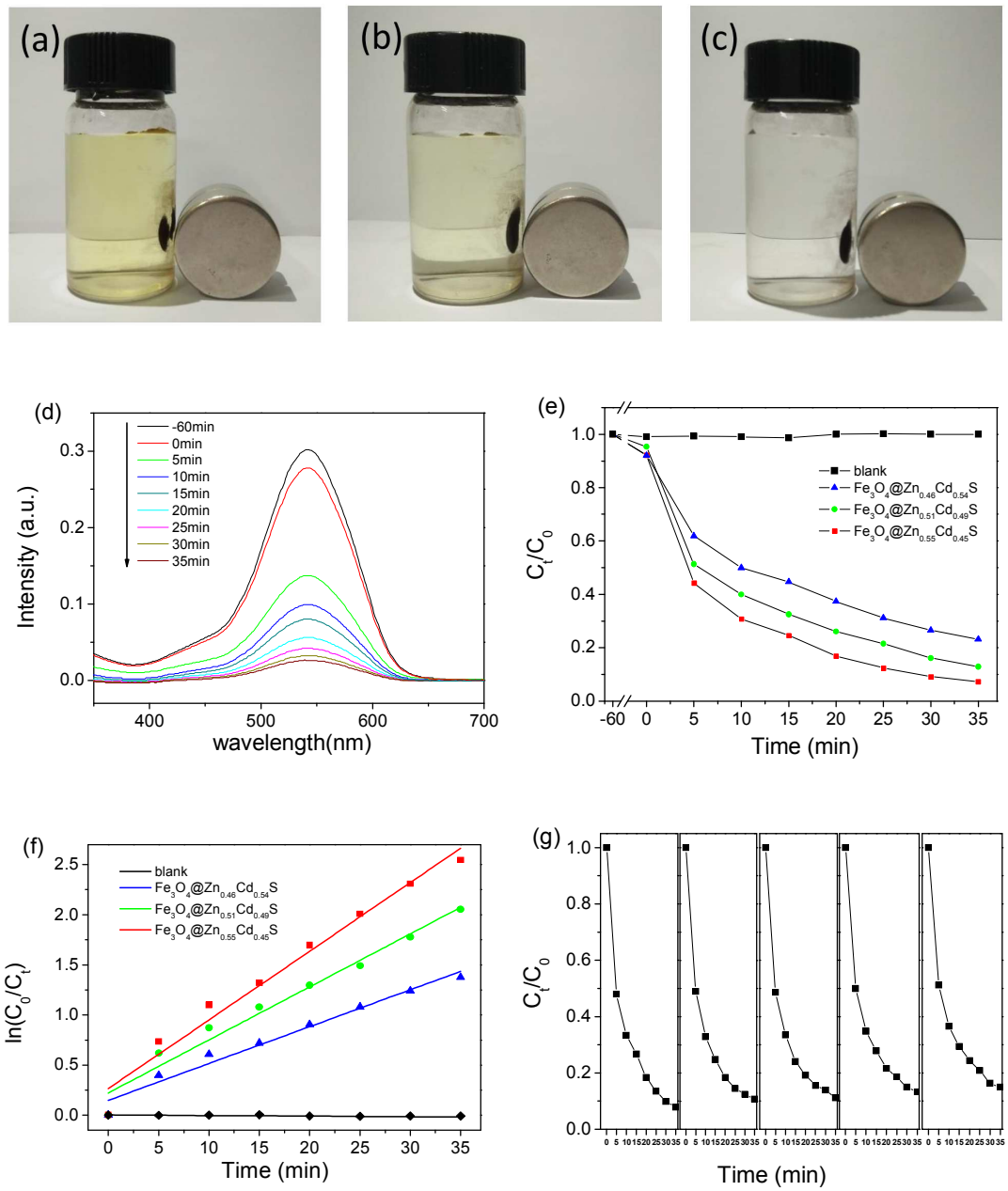

Figure 5. (a-c) Digital photos of Cr(VI) aqueous solution with Fe_3O_4@$Zn_{0.55}Cd_{0.45}S$ after irradiation of NIR light for 0, 10 and 35 min; (d) UV-Vis absorbance spectra of Cr(VI)-complex in presence of Fe_3O_4@$Zn_{0.55}Cd_{0.45}S$ microspheres under irradiation of 1500 mW Xe lamp for different time; (e, f) photochemical reduction and kinetic curves of Cr(VI) in presence of different Fe_3O_4@$Zn_xCd_{1-x}S$ under irradiation, C_0: the concentration of initial solution, C_t: the concentration at the irradiation time; (g) five recycling tests of photoreduction of Cr(VI) under irradiation for 35 min using 10 mg Fe_3O_4@$Zn_{0.55}Cd_{0.45}S$.

In fact, the photo-generated e^- as the sole reductive species, it can also react with Fe(III) in the interface of Fe_3O_4@$Zn_xCd_{1-x}S$ core-shell and also reduce O_2 to obtain·O^{2-}. To clarify the competitive relationship between the two reactions and some comparative experiments have been carried out to evaluate the influence of the reduction of Cr(VI) and the reduction between Fe(III) and e^-. As shown in Fig. S6, 7(in

the supporting information), the photochemical reduction and kinetic curves of Cr(VI) in presence of 10 mg Fe_3O_4, 10 mg $Zn_{0.43}Cd_{0.57}S$ as well as their mixture under irradiation show that $Zn_{0.55}Cd_{0.45}S$ microspheres exhibit excellent photocatalytic performance towards reduction of Cr(VI) and the catalytic efficiency of the photocatalysts has a slightly weaken in presence of Fe_3O_4, which can be attributed to possible reduction of Fe(III) by the photo-generated e^-

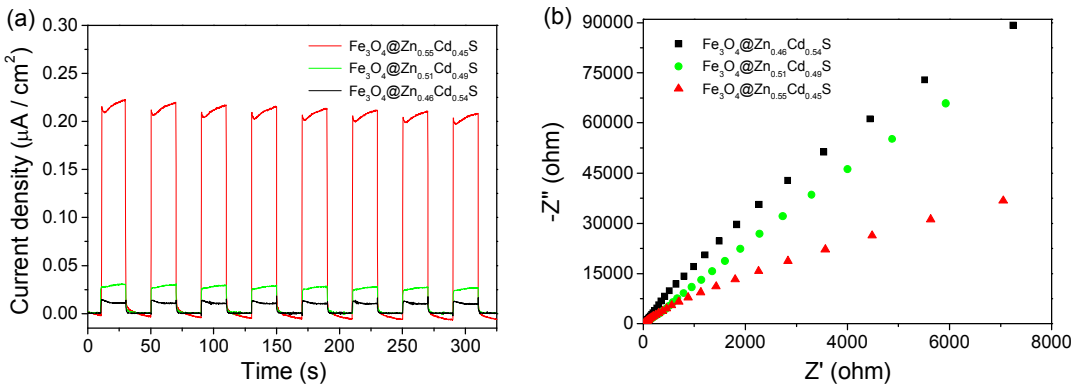

Figure 6. (a) Photocurrent responses and (b) impedance spectroscopy (EIS) of the as-prepared samples in dark.

4. Conclusions

In summary, magnetic recyclable Fe_3O_4@$Zn_xCd_{1-x}S$ core-shell microspheres have been prepared via the facile sacrificed-template technique under hydrothermal condition. The magnetic core-shell microspheres with tunable shell thickness have been obtained by adding different amount of $Cd(Ac)_2$ and thiourea in presence of Fe_3O_4@ZnS microspheres with different shell thickness. The as-prepared Fe_3O_4@$Zn_xCd_{1-x}S$ core-shell microspheres show good photochemical reduction ability towards Cr(VI) and oxidation photo-degradation ability towards of methylene blue dyes under irradiation of visible light. In addition, successive recycling experiments demonstrate that the as-prepared composite microspheres exhibit excellent chemical stability and recyclability, which is of great importance for practical applications.

Supporting Information

The Supporting Information is available free of charge on the ACS Publications website at DOI: .

Experimental procedure for hydroxyl radical (·OH) detection, fabrication of $Zn_{0.43}Cd_{0.57}S$ hollow microspheres and characterizations, TEM images (Figure S1, S3, S6), high-resolution XRD patterns (Figure S2), photo-oxidation of MB (Figure S4), fluorescence spectra (Figure S5), photochemical oxidation and removal kinetic curves (Figure S5), element composition and accurate mole ratio of Zn/Cd (Table S1, S2).

Acknowledgement. We acknowledge the funding supports from the National Natural Science Foundation of China (21471043) and Natural Science Foundation of Anhui Province (JZ2017AKZR0138). J. Zhang and W. Wang contributed to this work equally.

References

(1) Zhang, G. G.; Lan, Z. A.; Wang, X. C. Conjugated Polymers: Catalysts for Photocatalytic Hydrogen Evolution. *Angew. Chem. Int. Ed.* **2016**, *55*, 15712-15727.

(2) Shi, R.; Cao, Y. H.; Bao, Y. J.; Zhao, Y. F.; Waterhouse, G. I. N.; Fang, Z. Y, Wu, L. Z.; Tung, C. H.; Yin, Y. D.; Zhang, T. R. Self-Assembled Au/CdSe Nanocrystal Clusters for Plasmon-Mediated Photocatalytic Hydrogen Evolution. *Adv. Mater.* **2017**, *29*, 1700803.

(3) Chen, G. B.; Gao, R.; Zhao, Y. F.; Li, Z. H.; Waterhouse, G. I. N.; Shi, R.; Zhao, J. Q.; Zhang, M. T.; Shang L.; Sheng G. Y.; Zhang X. P.; Wen X. D.; Wu L. Z.; Tung C. H.; Zhang T. R. Alumina-Supported CoFe Alloy Catalysts Derived from Layered-Double-Hydroxide Nanosheets for Effcient Photothermal CO_2 Hydrogenation to Hydrocarbons. *Adv. Mater.* **2018**, *30*, 1704663.

(4) Yu, H. J.; Shi, R.; Zhao, Y. X.; Bian, T.; Zhao, Y. F.; Zhou, C.; Waterhouse, G. I. N.; Wu, L. Z.; Tung, C. H.; Zhang, T. R. Alkali-Assisted Synthesis of Nitrogen Defcient Graphitic Carbon Nitride with Tunable Band Structures for Effcient Visible-Light-Driven Hydrogen Evolution. *Adv. Mater.* **2017**, *29*, 1605148.

(5) Ran, J.; Gao, G.; Li, F. T.; Ma, T. Y.; Du, A.; Qiao, S. Z. Ti_3C_2 MXene Co-catalyst on Metal Sulfide Photo-Absorbers for Enhanced Visible-light Photocatalytic Hydrogen Production. *Nat. Commun.* **2017**, *8*, 13907.

(6) Huang, Z. F.; Song, J. J.; Li, K.; Tahir, M.; Wang, Y. T.; Pan, L.; Wang, L.; Zhang, X. W.; Zou, J. J. Hollow Cobalt-Based Bimetallic Sulfide Polyhedra for Efficient All-pH-Value Electrochemical and Photocatalytic Hydrogen Evolution. *J. Am. Chem. Soc.* **2016**, *138*, 1359-1365.

(7) Kudo, A.; Miseki, Y. Heterogeneous Photocatalyst Materials for Water Splitting. *Chem. Soc. Rev.* **2009**, *38*, 253-278.

(8) Chen, X. B.; Shen, S. H.; Guo, L. J.; Mao, S. S. Semiconductor-Based Photocatalytic Hydrogen Generation. *Chem. Rev.* **2010**, *110*, 6503-6570.

(9) He, B.; Liu, R.; Ren, J. B.; Tang, C. J.; Zhong, Y. J.; Hu, Y. One-Step Solvothermal Synthesis of Petalous Carbon-Coated Cu^+-Doped CdS Nanocomposites with Enhanced Photocatalytic Hydrogen Production. *Langmuir* **2017**, *33*, 6719-6726.

(10) Li, X.; Yu, J.; Jaroniec, M. Hierarchical Photocatalysts. *Chem. Soc. Rev.* **2016**, *45*, 2603-2636.

(11) Yu, C.; Li, G.; Kumar, S.; Yang, K.; Jin, R. Phase Transformation Synthesis of Novel Ag_2O/Ag_2CO_3 Heterostructures with High Visible Light Efficiency in Photocatalytic Degradation of Pollutants. *Adv. Mater.* **2014**, *26*, 892-898.

(12) Huang, H. W.; Han, X.; Li, X.W.; Wang, S. C.; Chu, P. K.; Zhang, Y. H. Fabrication of Multiple Heterojunctions with Tunable Visible-Light-Active Photocatalytic Reactivity in BiOBr-BiOI Full-Range Composites Based on Microstructure Modulation and Band Structures. *ACS Appl. Mater. Interf.* **2015**, *7*, 482-492.

(13) Boyjoo, Y.; Sun, H.; Liu, J.; Pareek, V. K.; Wang, S. B. A Review on Photocatalysis for Air Treatment: From Catalyst Development to Reactor Design. *Chem. Eng. J.* **2017**, *310*, 537-559.

(14) Huang, H. W.; Xiao, K.; Zhang, T. R.; Dong, F.; Zhang, Y. H. Rational Design on 3D Hierarchical Bismuth Oxyiodides via in situ Self-Template Phase Transformation and Phase-Junction Construction for Optimizing Photocatalysis against Diverse Contaminants. *Appl. Catal. B-Environ.* **2017**, *203*, 879-888.

(15) Habisreutinger, S. N.; Schmidt-Mende, L.; Stolarczyk J. K. Photocatalytic Reduction of CO_2 on TiO_2 and Other Semiconductors. *Angew. Chem. Int. Ed.* **2013**, *52*, 7372-7408.

(16) Huang, H. W.; He, Y.; Du, X.; Chu, P. K.; Zhang, Y. H. A General and Facile Approach to Heterostructured Core/Shell $BiVO_4$/BiOI p-n Junction: Room-Temperature in Situ Assembly and Highly Boosted Visible-Light Photocatalysis. *ACS Sustain Chem. Eng.* **2015**, *3*, 3262-3273.

(17) Wan, Z.; Zhang, G. K.; Wu, X. Y.; Yin, S. Novel Visible-Light-Driven Z-Scheme $Bi_{12}GeO_{20}$/g-C_3N_4 Photocatalyst: Oxygen-Induced Pathway of Organic Pollutants Degradation and Proton

Assisted Electron Transfer Mechanism of Cr(VI) Reduction. *Appl. Catal. B-Environ.* **2017**, *207*, 17-26.

(18) Huang, H.W.; Xiao, K.; He, Y.; Zhang, T. R.; Dong, F.; Du, X.; Zhang, Y. H. In situ Assembly of BiOI@$Bi_{12}O_{17}Cl_2$ p-n Junction: Charge Induced Unique Front-Lateral Surfaces Coupling Heterostructure with High Exposure of BiOI {001} Active Facets for Robust and Nonselective Photocatalysis. *Appl. Catal. B: Environ.* **2016**, *199*, 75-86.

(19) Meng, X. D.; Zhang, G. K.; Li, N. $Bi_{24}Ga_2O_{39}$ for Visible Light Photocatalytic Reduction of Cr(VI): Controlled Synthesis, Facet-Dependent Activity and DFT Study. *Chem. Eng. J.* **2017**, *314*, 249-256.

(20) Ong, W. J.; Tan, L. L.; Ng, Y. H.; Yong, S. T.; Chai, S. P. Graphitic Carbon Nitride (g-C_3N_4)-Based Photocatalysts for Artificial Photosynthesis and Environmental Remediation: Are We a Step Closer To Achieving Sustainability? *Chem. Rev.* **2016**, *116*, 7159-7329.

(21) Schultz, D. M.; Yoon, T. P. Solar Synthesis: Prospects in Visible Light Photocatalysis. *Science* **2014**, *343*, 1239176.

(22) Zhao, Y. F.; Zhao, Y. X.; Waterhouse, G. I. N.; Zheng, L. R.; Cao, X. Z.; Teng, F.; Wu, L. Z.; Tung, C. H.; O'Hare, D.; Zhang, T. R. Layered-Double-Hydroxide Nanosheets as Effcient Visible-Light-Driven Photocatalysts for Dinitrogen Fixation. *Adv. Mater.* **2017**, *29*, 1703828.

(23) Low, J.; Yu, J.; Jaroniec, M.; Wageh, S.; Al-Ghamdi, A. A. Heterojunction Photocatalysts. *Adv. Mater.* **2017**, *29*, 1601694.

(24) Zhao, Y. F.; Zhao, B.; Liu, J. J.; Chen, G. B., Gao, R.; Yao, S. Y.; Li, M. Z.; Zhang, Q. H.; Gu, L.; Xie, J. L.; Wen, X. D.; Wu, L. Z.; Tung, C. H.; Ma, D.; Zhang, T. R. Oxide-Modified Nickel Photocatalysts for the Production of Hydrocarbons in Visible Light. *Angew. Chem. Int. Ed.* **2016**, *55*, 4215-4219.

(25) Gómez-Pastora, J.; Dominguez, S.; Bringas, E.; Rivero, M. J.; Ortiz, I.; Dionysiou, D. D. Review and Perspectives on the Use of Magnetic Nanophotocatalysts (MNPCs) in Water Treatment. *Chem. Eng. J.* **2017**, *310*, 407-427.

(26) Rossi, L. M.; Costa, N. J. S.; Silva, F. P.; Wojcieszak, R. Magnetic Nanomaterials in Catalysis: Advanced Catalysts for Magnetic Separation and Beyond. *Green Chem.* **2014**, *16*, 2906.

(27) Sharma, R. K.; Dutta, S.; Sharma, S.; Zboril, R.; Varma, R. S.; Gawande, M. B. Fe_3O_4 (Iron Oxide)-Supported Nanocatalysts: Synthesis, Characterization and Applications in Coupling Reactions. *Green Chem.* **2016**, *18*, 3184-3209.

(28) Wu, W.; Changzhong, J.; Roy, V. A. Recent Progress in Magnetic Iron Oxide-Semiconductor Composite Nanomaterials as Promising Photocatalysts. *Nanoscale* **2015**, *7*, 38-58.

(29) Gawande, M. B.; Branco, P. S.; Varma, R. S. Nano-Magnetite (Fe_3O_4) as A Support for Recyclable Catalysts in the Development of Sustainable Methodologies. *Chem. Soc. Rev.* **2013**, *42*, 3371-3393.

(30) Pang, F.; Zhang, R.; Lan, D.; Ge, J. Synthesis of Magnetite-Semiconductor-Metal Trimer Nanoparticles through Functional Modular Assembly: A Magnetically Separable Photocatalyst with Photothermic Enhancement for Water Reduction. *ACS Appl. Mater. Interfaces* **2018**, *10*, 4929-4936.

(31) Lin, F. H.; Doong, R. A. Bifunctional Au-Fe_3O_4 Heterostructures for Magnetically Recyclable Catalysis of Nitrophenol Reduction. *J. Phys. Chem. C* **2011**, *115*, 6591-6598.

(32) Shang, L.; Liang, Y. H.; Li, M. Z.; Waterhouse, G. I. N.; Tang, P.; Ma, D.; Wu, L. Z.; Tung, C. H.; Zhang, T. R. "Naked" Magnetically Recyclable Mesoporous Au-γ-Fe_2O_3 Nanocrystal Clusters: A Highly Integrated Catalyst System. *Adv. Funct. Mater.* **2017**, *27*, 1606215.

(33) Zhu, M. Y.; Wang, C. J.; Meng, D. H.; Diao, G. W. In Situ Synthesis of Silver Nanostructures on Magnetic Fe_3O_4@ C Core–Shell Nanocomposites and Their Application in Catalytic Reduction Reactions. *J. Mater. Chem. A* **2013**, *1*, 2118-2125.

(34) Zhu, Z.; Lu, Z. Y.; Wang, D. D.; Tang, X.; Yan, Y. S.; Shi, W. D.; Wang, Y. S.; Gao, N. L.; Yao, X.; Dong, H. J. Construction of High-Dispersed Ag/Fe_3O_4/g-C_3N_4 Photocatalyst by Selective Photo-Deposition and Improved Photocatalytic Activity. *Appl. Catal. B-Environ.* **2016**, *182*, 115-122.

(35) Wu, S. X.; He, Q. Y.; Zhou, C. M.; Qi, X. Y.; Huang, X.; Yin, Z. Y.; Yang, Y. H.; Zhang, H. Synthesis of Fe_3O_4 and Pt Nanoparticles on Reduced Graphene Oxide and Their Use as A Recyclable Catalyst. *Nanoscale* **2012**, *4*, 2478-2483.

(36) Wang, C.; Daimon, H.; Sun, S. H. Dumbbell-Like Pt-Fe_3O_4 Nanoparticles and Their Enhanced Catalysis for Oxygen Reduction Reaction, *Nano Lett.* **2009**, *9*, 1493-1496.

(37) Li, X. Y.; Wang, X.; Song, S. Y.; Liu, D. P.; Zhang, H. J. Selectively Deposited Noble Metal Nanoparticles on Fe_3O_4/Graphene Composites: Stable, Recyclable, and Magnetically Separable Catalysts. *Chem. Eur. J.* **2012**, *18*, 7601-7607.

(38) Elazab, H. A.; Siamaki, A. R.; Moussa, S.; Gupton, B. F.; El-Shall, M. S. Highly Efficient and Magnetically Recyclable Graphene-Supported Pd/Fe_3O_4 Nanoparticle Catalysts for Suzuki and Heck Cross-Coupling Reactions. *Appl. Catal. A-Gen.* **2015**, *491*, 58-69.

(39) Zubir, N. A.; Yacou, C.; Motuzas ,J.; Zhang, X. W.; Zhao, X. S.; da Costa, J. C. D. The Sacrificial Role of Graphene Oxide in Stabilising a Fenton-Like Catalyst GO-Fe_3O_4. *Chem. Commun.* **2015**, *51*, 9291-9293.

(40) Yang, J.; Zhu, G. X.; Liu, Y. J.; Xia, J. X.; Ji, Z. Y.; Shen, X. P.; Wu, S. K. Fe_3O_4-Decorated Co_9S_8 Nanoparticles In Situ Grown on Reduced Graphene Oxide: A New and Efficient Electrocatalyst for Oxygen Evolution Reaction. *Adv. Funct. Mater.* **2016**, *26*, 4712-4721.

(41) Atarod, M.; Nasrollahzadeh, M.; Mohammad-Sajadi, M. Green Synthesis of Pd/RGO/Fe_3O_4 Nanocomposite Using Withania Coagulans Leaf Extract and Its Application as Magnetically

Separable and Reusable Catalyst for the Reduction of 4-Nitrophenol. *J. Colloid Interface Sci.* **2016**, *465*, 249-258.

(42) Zhang, C. F.; Qiu, L. G.; Ke, F.; Zhu, Y. J.; Yuan, Y. P.; Xu, G. S.; Jiang, X. A Novel Magnetic Recyclable Photocatalyst Based on A Core-Shell Metal-Organic Framework Fe_3O_4@ MIL-100 (Fe) for the Decolorization of Methylene Blue Dye. *J. Mater. Chem. A* **2013**, *1*, 14329-14334.

(43) Zhang, Y. F.; Qiu, L. G.; Yuan, Y. P.; Zhu, Y. J.; Jiang, X.; Xiao, J. D. Magnetic Fe_3O_4@C/Cu and Fe_3O_4@CuO Core-Shell Composites Constructed from MOF-Based Materials and Their Photocatalytic Properties under Visible Light. *Appl. Catal. B-Environ.* **2014**, *144*, 863-869.

(44) Ke, F.; Wang, L. H.; Zhu, J. F. Multifunctional Au-Fe_3O_4@ MOF Core–Shell Nanocomposite Catalysts with Controllable Reactivity and Magnetic Recyclability. *Nanoscale* **2015**, *7*, 1201-1208.

(45) Elsaidi, S. K.; Sinnwell, M. A.; Banerjee, D.; Devaraj, A.; Kukkadapu, R. K.; Droubay, T. C.; Nie, Z. M.; Kovarik, L.; Vijayakumar, M.; Manandhar, S. Reduced Magnetism in Core-Shell Magnetite@MOF Composites. *Nano Lett.* **2017**, *17*, 6968-6973.

(46) Chalasani, R.; Vasudevan, S. Cyclodextrin-Functionalized Fe_3O_4@TiO_2: Reusable, Magnetic Nanoparticles for Photocatalytic Degradation of Endocrine-Disrupting Chemicals in Water Supplies. *ACS Nano* **2013**, *7*, 4093-4104.

(47) Yu, X. X.; Liu, S. W.; Yu, J. G. Superparamagnetic γ-Fe_2O_3@SiO_2@TiO_2 Composite Microspheres with Superior Photocatalytic Properties. *Appl. Catal. B-Environ.* **2011**, *104*, 12-20.

(48) Subramonia, W.; Wu, T. Y.; Chai, S. P. Photocatalytic Degradation of Industrial Pulp and Paper Mill Effluent Using Synthesized Magnetic Fe_2O_3-TiO_2: Treatment Efficiency and Characterizations of Reused Photocatalyst. *J. Environ. Manage.* **2017**, *187*, 298-310.

(49) Li, W.; Deng, Y.; Wu, Z.; Qian, X.; Yang, J.; Wang, Y., Gu, D.; Zhang, F.; Tu, B.; Zhao, D. Hydrothermal Etching Assisted Crystallization: A Facile Route to Functional Yolk-Shell Titanate Microspheres with Ultrathin Nanosheets-Assembled Double Shells. *J. Am. Chem. Soc.* **2011**, *133*, 15830-15833.

(50) Xi, G. C.; Yue, B.; Cao, J. Y.; Ye, J. H. Fe_3O_4/WO_3 Hierarchical Core-Shell Structure: High-Performance and Recyclable Visible-Light Photocatalysis. *Chem. Eur. J.* **2011**, *17*, 5145-5154.

(51) Wang, L.; Wei, H. W.; Fan, Y. J; Gu, X.; Zhan, J. H. One-Dimensional CdS/α-Fe_2O_3 and CdS/Fe_3O_4 Heterostructures: Epitaxial and Nonepitaxial Growth and Photocatalytic Activity. *J. Phys. Chem. C* **2009**, *113*, 14119-14125.

(52) Shi, W.; Du, D.; Shen, B.; Cui, C. F.; Lu, L. J.; Wang, L. Z.; Zhang, J. L. Synthesis of Yolk–Shell Structured Fe_3O_4@void@CdS Nanoparticles: A General and Effective Structure Design for Photo-Fenton Reaction. *ACS Appl. Mater. Interfaces* **2016**, *8*, 20831-20838.

(53) Lin, T. R.; Wang, J.; Guo, L. Q.; Fu, F. F. Fe_3O_4@MoS_2 Core–Shell Composites: Preparation, Characterization, and Catalytic Application. *J. Phys. Chem. C* **2015**, *119*, 13658-13664.

(54) Mousavi, M.; Habibi-Yangjeh, A. Magnetically Separable Ternary g-C_3N_4/Fe_3O_4/BiOI Nanocomposites: Novel Visible-Light-Driven Photocatalysts Based on Graphitic Carbon Nitride. *J. Colloid Interface Sci.* **2016**, *465*, 83-92.

(55) Kumar, S.; Kumar, B.; Baruah, A.; Shanker, V. Synthesis of Magnetically Separable and Recyclable g-C_3N_4-Fe_3O_4 Hybrid Nanocomposites with Enhanced Photocatalytic Performance under Visible-Light Irradiation. *J. Phys. Chem. C* **2013**, *117*, 26135-26143.

(56) Habibi-Yangjeh, A.; Akhundi, A. Novel Ternary g-C_3N_4/Fe_3O_4/Ag_2CrO_4 Nanocomposites: Magnetically Separable and Visible-Light-Driven Photocatalysts for Degradation of Water Pollutants. *J. Mol. Catal. A-Chem.* **2016**, *415*, 122-130.

(57) Lu, Z. Y.; Zhao, X. X.; Zhu, Z.; Yan, Y. S.; Shi, W. D.; Dong, H. J.; Ma, Z. F.; Gao, N. L.; Wang, Y. S.; Huang, H. Enhanced Recyclability, Stability, and Selectivity of CdS/C@Fe_3O_4 Nanoreactors for Orientation Photodegradation of Ciprofloxacin. *Chem. Eur. J.* **2015**, *21*, 18528-18533.

(58) Li, N.; Zhang, J.; Tian, Y.; Zhao, J. H.; Zhang, J.; Zuo, W. Precisely Controlled Fabrication of Magnetic 3D γ-Fe_2O_3@ZnO Core-Shell Photocatalyst with Enhanced Activity: Ciprofloxacin Degradation and Mechanism Insight. *Chem. Eng. J.* **2017**, *308*, 377-385.

(59) Du, D.; Shi, W.; Wang, L. Z.; Zhang, J. L. Yolk-Shell Structured Fe_3O_4@void@TiO_2 as A Photo-Fenton-Like Catalyst for the Extremely Efficient Elimination of Tetracycline. *Appl. Catal. B-Environ.* **2017**, *200*, 484-492.

(60) Li, Q.; Meng, H.; Zhou, P.; Zheng, Y. Q.; Wang, J.; Yu, J. G.; Gong, J. R. $Zn_{1-x}Cd_xS$ Solid Solutions with Controlled Bandgap and Enhanced Visible-Light Photocatalytic H_2-Production Activity. *ACS Catal.* **2013**, *3*, 882-889.

(61) Xu, X.; Lu, R. J.; Zhao, X. F.; Xu, S. L.; Lei, X. D.; Zhang, F. Z.; Evans, D. G. Fabrication and Photocatalytic Performance of A $Zn_xCd_{1-x}S$ Solid Solution Prepared by Sulfuration of A Single Layered Double Hydroxide Precursor. *Appl. Catal. B-Environ.* **2011**, *102*, 147-156.

(62) Meng, S. G.; Ye, X. J.; Ning, X. F.; Xie, M. L.; Fu, X. L.; Chen, S. F. Selective Oxidation of Aromatic Alcohols to Aromatic Aldehydes by BN/Metal Sulfide with Enhanced Photocatalytic Activity. *Appl. Catal. B-Environ.* **2016**, *182*, 356-368.

(63) Chen, Y.; Zhao, S.; Wang, X.; Peng, Q.; Lin, R.; Wang, Y.; Shen, R.; Cao, X.; Zhang, L.; Zhou, G.;Li, J.; Xia, A.; Li, Y. Synergetic Integration of $Cu_{1.94}S$-$Zn_xCd_{1-x}S$ Heteronanorods for Enhanced Visible-Light-Driven Photocatalytic Hydrogen Production. *J. Am. Chem. Soc.* **2016**, *138*, 4286-4289.

(64) Zhao, H.; Ding, X. L.; Zhang, B.; Li, Y. X.; Wang, C. Y. Enhanced Photocatalytic Hydrogen Evolution along with Byproducts Suppressing over Z-scheme $Cd_xZn_{1-x}S$/Au/g-C_3N_4 Photocatalysts under Visible Light. *Sci. Bull.*, **2017**, *62*,602-609.

(65) Su, Y.; Zhang, Z.; Liu, H.; Wang, Y. $Cd_{0.2}Zn_{0.8}S$@UiO-66-NH_2 Nanocomposites as Efficient and Stable Visible-Light-Driven Photocatalyst for H_2 Evolution and CO_2 Reduction. *Appl. Catal. B-Environ.* **2017**, *200*, 448-457.

(66) Hu, J. L.; Yang, Q. H.; Lin, H.; Ye, Y. P.; He, Q.; Zhang, J. N.; Qian, H. S. Mesoporous Silica Nanospheres Decorated with CdS Nanocrystals for Enhanced Photocatalytic and Excellent Antibacterial Activities. *Nanoscale* **2013**, *5*, 6327-6332.

(67) Xu, X.; Deng, C.; Ga, M.; Yu, W.; Yang, P.; Zhang, X. Synthesis of Magnetic Microspheres with Immobilized Metal Ions for Enrichment and Direct Determination of Phosphopeptides by Matrix-Assisted Laser Desorption Ionization Mass Spectrometry. *Adv. Mater.* **2006**, *18*, 3289-3293.

(68) Zhang, F.; Wang, W. N.; Cong, H. P.; Luo, L. B.; Zha, Z. B.; Qian, H. S. Facile Synthesis of Upconverting Nanoparticles/Zinc Oxide Core–Shell Nanostructures with Large Lattice Mismatch for Infrared Triggered Photocatalysis. *Part. Part. Syst. Charact.* **2017**, *34*, 1600222.

(69) Wang, W. N.; Huang, C. X.; Zhang, C. Y.; Zhao, M. L.; Zhang, J.; Chen, H. J.; Zha, Z B.; Zhao T.; Qian H. S. Controlled Synthesis of Upconverting Nanoparticles/$Zn_xCd_{1-x}S$ Yolk-Shell Nanoparticles for Efficient Photocatalysis Driven by NIR Light. *Appl. Catal. B-Environ.* **2018**, *224*, 854-862.

(70) Zhao, M. L.; Wang, W. N.; Huang, C. X.; Dong, W.; Wang, Y.; Cheng, S.; Wang, H. Q.; Qian, H. S. Facile Synthesis of UCNPs/$Zn_xCd_{1-x}S$ Nanocomposites Excited by Near-Infrared Light for Photochemical Reduction and Removal of Cr(VI). *Chin. J. Catal.* **2018**, *39*, 1240-1248.

(71) Deng, H.; Li X. L., Peng, Q.; Wang, X.; Chen, J. P; Li, Y. D. Monodisperse Magnetic Single-Crystal Ferrite Microspheres. *Angew. Chem. Int. Ed.* **2005**, *117*, 2842-2845.

(72) Chen, J.; Ding, B. B.; Wang, T. Y.; Li, F.; Zhang, Y.; Zhao, Y. L.; Qian, H. S. Facile Synthesis of Uniform $Zn_xCd_{1-x}S$ Alloyed Hollow Nanospheres for Improved Photocatalytic Activities. *J. Mater. Sci-Mater. El.* **2014**, *25*, 4103-4109.

(73) Gao, X. H.; Wu, H. B.; Zheng, L. X.; Zhong, Y. J.; Hu, Y.; Lou, X. W. Formation of Mesoporous Heterostructured $BiVO_4/Bi_2S_3$ Hollow Discoids with Enhanced Photoactivity. *Angew. Chem. Int. Ed.* **2014**, *126*, 6027-6031.

(74) Wang, X.; Liang, Y. H.; An, W. J.; Hu, J. S.; Zhu, Y. F.; Cui, W. Q. Removal of Chromium (VI) by A Self-Regenerating and Metal Free g-C_3N_4/Graphene Hydrogel System via the Synergy of Adsorption and Photo-Catalysis under Visible Light. *Appl. Catal. B-Environ.* **2017**, *219*, 53-62.

(75) Wang, H.; Jiang, S. L.; Shao, W.; Zhang, X. D.; Chen, S. C.; Sun, X. S.; Zhang, Q.; Luo, Y.; Xie, Y. Optically Switchable Photocatalysis in Ultrathin Black Phosphorus Nanosheets. *J. Am. Chem. Soc*. **2018**, *140*, 3474-3480.

(76) Zhu, Y. Y.; Wang, Y. J.; Ling, Q.; Zhu, Y. F. Enhancement of Full-Spectrum Photocatalytic Activity over $BiPO_4/Bi_2WO_6$ Composites. *Appl. Catal. B-Environ.***2017**, *200*, 222-229.

(77) Huang, H. W.; Tu, S. C.; Zeng, C.; Zhang, T. R.; Reshak, A. H.; Zhang, Y. H. Macroscopic Polarization Enhancement Promoting Photo- and Piezoelectric-Induced Charge Separation and Molecular Oxygen Activation. *Angew. Chem.* **2017**, *129*, 12022-12026.

(78) Huang, H. W.; Li, X. W.; Wang, J. J.; Dong, F.; Chu, P. K.; Zhang, T. R.; Zhang, Y. H. Anionic Group Self-Doping as a Promising Strategy: Band-Gap Engineering and Multi-Functional Applications of High-Performance CO_3^{2-}-Doped $Bi_2O_2CO_3$. *ACS Catal.* **2015**, *5*, 4094-4103.

(79) Huang, H. W.; He, Y.; Li, X. W.; Li, M.; Zeng, C.; Dong, F.; Du, X.; Zhang, T. R.; Zhang, Y. H. $Bi_2O_2(OH)(NO_3)$ as A Desirable $[Bi_2O_2]^{2+}$ Layered Photocatalyst: Strong Intrinsic Polarity, Rational Band Structure and {001} Active Facets Co-Beneficial for Robust Photooxidation Capability. *J. Mater. Chem. A,* **2015**, *3*, 24547-24556.

Graphic abstract:

Magnetically recyclable Fe_3O_4@$Zn_xCd_{1-x}S$ core-shell microspheres have been fabricated successfully via a facile sacrificed-template assisted hydrothermal approach for photochemical reduction of Cr(VI) and oxidation of organic dyes under irradiation of visible light.